Arch. Metall. Mater. **69** (2024), 1, 181-187

DOI: https://doi.org/10.24425/amm.2024.147807

QIAOLI WANG[1,2†], YINAN XIAO[2†], DI WU[2], FANG YANG[3], L.Y. SHENG[1,2*]

MICROSTRUCTURE, COMPRESSIVE PROPERTIES AND OXIDATION BEHAVIORS OF THE Nb-Si-Ti-Cr-Al-Ta-Hf ALLOY WITH MINOR HOLMIUM ADDITION

In the present research, the Nb-Si-Ti-Cr-Al-Ta-Hf alloys with different Ho addition were prepared. Their microstructure, compressive properties and oxidation behaviors were investigated preliminarily. The results exhibit that the Nb-Si-Ti-Cr-Al-Ta-Hf alloy has coarse microstructure which is mainly composed of Nb solid solution, Nb_5Si_3 and Ti_5Si_3 phases. The minor Ho addition could refine the microstructure and suppress the precipitation of Ti_5Si_3 phase. Moreover, the Ho addition also leads to the formation of $Ho_2Hf_2O_7$, which prefers to precipitate along the Nbss/Nb_5Si_3 phase interface. Compared with the Nb-Si-Ti-Cr-Al-Ta-Hf alloy, the minor Ho addition improves the room-temperature and high-temperature compressive properties of the alloy. Its room-temperature compressive strength and ductility obtain the maximum value of 1825 MPa and 16.5% when the Ho content is 0.1 at.%. Moreover, its best compressive strength at 873 K, 1273 K and 1473 K is 1495 MPa, 765 MPa and 380 MPa, respectively, when the Ho addition is 0.1 at.%. The oxidation behavior of the Nb-Si-Ti-Cr-Al-Ta-Hf alloy is diversified with the Ho addition. The oxidation rate of the alloy with 0.1 at.% Ho addition is the lowest while the alloy with 0.2 at.% Ho addition is the highest. Therefore, the 0.1 at.% Ho would be the appropriate content for the Nb-Si-Ti-Cr-Al-Ta-Hf alloy.

Keywords: Nb alloy; Nb_5Si_3 phase; Microstructure; Mechanical properties; Oxidation behavior

1. Introduction

In the few decades, intermetallic compounds have been paid great attention, since their excellent properties such as high structural stability, high strength, good thermal conductivity, and so on [1-4]. Especially in the aerospace, power, metallurgy industries, the increasing of working temperature has put forward higher requirements on the materials used as the high-temperature component [5,6]. Now, one method is fabrication the thermal barrier coatings with better performance, but their improvement is limited, due to the interface cracking [7,8]. The other method is developing the new materials with better high-temperature strength, better creep properties and good oxidation resistance [9,10]. As one typical intermetallic compounds, the niobium silicide (NbSi) has attracted more attention, because its ultrahigh melting point and excellent creep resistance [11,12]. Therefore, the NbSi based alloy has been considered as the most potential material to develop the new blade for high performance gas turbine [13]. However, the long range ordered structure of the NbSi phase makes it intrinsic brittleness, which is detrimental to its room-temperature ductility [14]. Moreover, the "pest" oxidation of Nb based alloy also restricts its application at high temperature [15]. Then, improving the room-temperature strength and oxidation resistance of the NbSi based alloy have become a critical issue before its application.

Among the methods to improve the properties of NbSi based alloy, the alloying has been considered as the most convenient and effective one. Especially for the intrinsic brittleness of NbSi intermetallic compound, the introducing of ductile phase is a feasible way. Recently, the researches [16,17] have improved the room-temperature mechanical properties of NbSi based alloy by microstructure optimization, which demonstrates the benefit of incorporated ductile phase on fracture toughness. The researches on Nb-Si alloy revealed that the doped Hf and Ti helped the formation of Nb_3Si phase and the Cr and Al addition contributed the formation of Nb_5Si_3 phase [18,19]. However, Grammenos et al [20] studied the effect of Al, Cr and Ti addition on the microstructure of Nb-18Si-5Hf alloy and indicated that Ti could stabilize the Nb_5Si_3 phase and promote the formation of lamellar structure. Actually, the increased alloying elements

[1] PEKING UNIVERSITY, SHENZHEN INSTITUTE, SHENZHEN 518057, CHINA
[2] PKU-HKUST SHENZHEN-HONGKONG INSTITUTION, SHENZHEN 518057, CHINA
[3] SHENZHEN AIRLINES, SHENZHEN BAO'AN INTERNATIONAL AIRPORT, SHENZHEN 518128, CHINA

* Corresponding author: lysheng@yeah.net

† These authors contributed equally to this work

would result in the phase transformation and precipitation along interface, which influences its high-temperature strength [21]. In addition, for the multi-phase alloy, how to take full use of the ductile phase and stiffness phase is another important factor that greatly affects the mechanical properties. The researches on multi-phase alloys with intermetallic compound indicated that the Rare Earth (RE) could refine the microstructure and contribute to the strength and ductility simultaneously [22,23]. Moreover, the added RE can purify the grain boundary by arresting the oxygen and impurities, which benefits the fracture toughness [2,24]. Then, it can be anticipated that the appropriate RE addition, cooperated with other alloying element, could improve the properties of the NbSi alloy effectively.

Therefore, in the present research, the Nb-Si-Ti-Cr-Al-Ta-Hf alloys with minor addition of holmium (Ho) was fabricated by conventional method. The microstructure, phase constituent, compressive properties and oxidation behavior of the alloys were investigated to demonstrate the appropriate Ho addition.

2. Experimental procedures

The Nb-Si-Ti-Cr-Al-Ta-Hf alloys with different Ho contents were prepared by the vacuum arc furnace with the definite composition, as shown in TABLE 1. The pure metals of niobium (99.9%), silicon (99.9%), titanium (99.9%), chromium (99.9%), aluminum (99.9%), tantalum (99.9%), hafnium (99.8%) and holmium (99.7%) were arc-melted in a water-cooled copper crucible. The alloy buttons were turned over and remelted for five times to homogenize the chemical composition. Due to the elemental losses were almost less than 0.5% in mass, the nominal compositions of the alloys were considered as their real composition.

TABLE 1

Nominal compositions of Nb-Si-Ti-Cr-Al-Ta-Hf alloys with different Ho addition (at.%)

Alloy	Ho	Hf	Ta	Al	Cr	Ti	Si	Nb
0Ho	0	2	2	3	6	22	16	49
0.1Ho	0.1	2	2	3	6	22	16	48.9
0.2Ho	0.2	2	2	3	6	22	16	48.8

The specimens for scanning electron microscopy (SEM) and X-ray diffractometer (XRD) analyses were prepared by conventional metallographic techniques. The SEM S3400 with energy disperse spectroscopy (EDS) were employed to characterize the microstructure and phase content. The detailed phase constituents were analyzed by the Bruker D8 Advance XRD with Cu-Ka radiation (λ = 0.15418 nm) at 40 kV and 40 mA. The specimens for transmission electron microscopy (TEM) observation were cut from the alloys and then ground. The final specimens with diameter of 3 mm and thickness of 25 μm were twin-jet electropolished in a solution of 10% perchloric acid and 90% alcohol at −20°C with the twin-jet current of 40 mA. The TEM observation was observed on JEOL-2100 to characterize the crystal structure and defects.

Rectangular compression specimens with the dimensions of 4 mm × 4 mm × 6 mm were cut from the buttons by electro-discharge machining (EDM) and the major surfaces were mechanically ground with 600-grit SiC abrasive prior to compression test. The compression tests were conducted in air using a Gleeble 1500 testing machine with an initial strain rate of 1×10^{-3} s^{-1} and the recorded load-time curves were converted to true stress-strain curves by taking constant volume into account.

The specimens for oxidation tests were cut from the alloys with the dimension of 10 mm × 10 mm × 3 mm and ground with 2000-grit SiC abrasive. The oxidation tests were performed in an open-ended tube furnace at 1100°C. Each specimen was placed in a separate alumina crucible during the test. The specimens were removed from the furnace at the intervals of 2, 3, 5, 10, 25, 40, and 60 h and weighed together with the crucible using a precision analytical balance (Model CPA225D, Germany) with an accuracy of 0.00001 g. The oxidized surfaces of the specimens were observed by the SEM S-3400. The phase constituents of the oxides were analyzed by the XRD.

3. Results and discussion

3.1. Microstructure and phase structure

The SEM observations on Nb-Si-Ti-Cr-Al-Ta-Hf alloys with and without Ho addition have been shown in Fig. 1. Clearly, the alloy mainly comprises three kinds of phases. In the Nb-Si-Ti-Cr-Al-Ta-Hf alloy without Ho addition, the gray-white Nb solid solution (Nbss) is the matrix embellished with coarse gray Nb_5Si_3 phases and relative small black Ti_5Si_3 phases, as shown in Fig. 1(a). Moreover, the Nbss and Nb_5Si_3 phases have formed the eutectic structure in some regions. With the addition of 0.1 at.% Ho, the microstructure becomes fine and demonstrates the near-eutectic morphology, as shown in Fig. 1(b). Though the

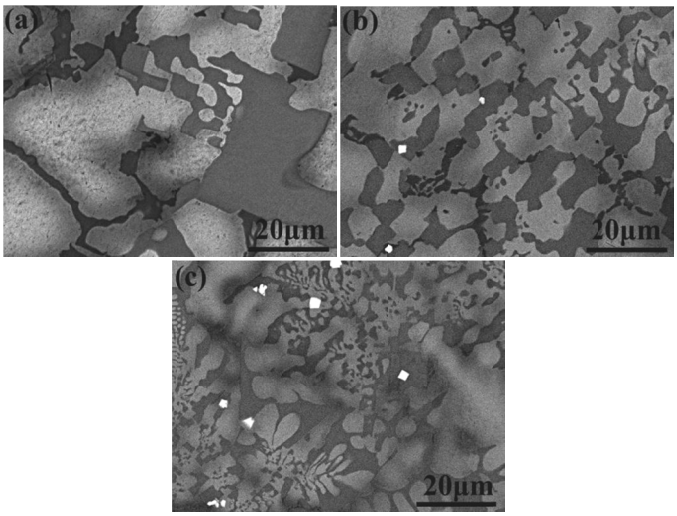

Fig. 1. Microstructures of Nb-Si-Ti-Cr-Al-Ta-Hf alloys with different Ho addition: (a) 0 Ho, (b) 0.1 Ho, (c) 0.2 Ho

distribution of Ti_5Si_3 phases is more homogeneous, the amount tends to decrease a little. In addition, some white phase can be observed along the Nbss and Nb_5Si_3 phase interface. The EDS test shows the white phase is rich of Hf, Ho and O, which indicates it should be the oxides of Hf and Ho. When the Ho addition is increased to 0.2 at.%, the microstructrual refinement is more distinct, which promotes some Nbss/Nb_5Si_3 lamellar eutectic structure, as shown in Fig. 1(c). Furthermore, the quantity of white phase is increased but their size almost changes little, compared with the 0.1 at.% Ho doped alloy.

The XRD has been employed to analyze the phase constituent in the Nb-Si-Ti-Cr-Al-Ta-Hf alloys with different Ho addition and the results are shown in Fig. 2. It can be found that the Nbss and Nb_5Si_3 are the main phases in all alloys, but the Ho addition has resulted in the phase evolution. Compared with the Nb-Si-Ti-Cr-Al-Ta-Hf alloy, the Ho addition has restrained the formation of Nb_5Si_3 phase. Especially in the 0.2 at.% Ho doped alloy, the diffraction peaks strength of the Nb_5Si_3 phase have decreased obviously. In addition, the Ho addition has led to the little deviation of Nbss diffraction peaks, which indicates it has caused lattice parameters changing in Nbss phase. Comparatively, the diffraction peak strength of Ti_5Si_3 phase has decreased greatly with the Ho addition. The diffraction peak evolution of XRD patterns has confirmed the microstructural observations.

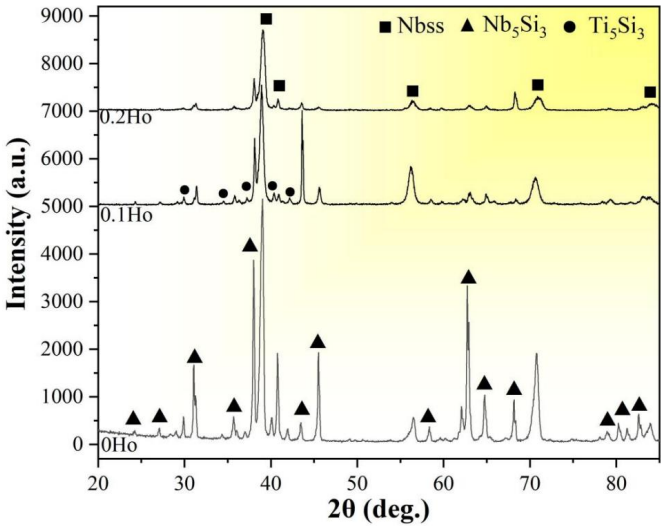

Fig. 2. XRD patterns of the Nb-Si-Ti-Cr-Al-Ta-Hf alloys with different Ho addition

To further study the phase and crystal feature, the TEM observations have been performed on the 0.2 at.% Ho doped Nb-Si-Ti-Cr-Al-Ta-Hf alloy. The bright-field TEM observation on the matrix reveals the fine eutectic structure, as shown in Fig. 3(a). Clearly, the Nb_5Si_3 phases have precipitated in the Nbss matrix with the ultrafine lamellar structure. The inset selected area electron diffraction (SAED) pattern indicates the Nb_5Si_3 phase has the tetragonal crystal structure with $a = b = 0.657$ nm and $c = 1.1887$ nm and I4/mcm space group. That means the Nb_5Si_3 phase has not preserve its high-temperature crystal structure. The high-resolution TEM observation on the Nbss/Nb_5Si_3 phase interface revels that there is a transition layer with about ten layer atoms, as shown in Fig. 3(b). Such a phase interface indicates the effect of lattice parameter difference between Nbss and Nb_5Si_3 phases [25]. Further TEM observation also find the Hf and Ho oxide in the Nbss phase, as show in Fig. 3(c). The selected area electron diffraction (SAED) pattern shows the oxide has the cubic crystal structure with $a = b = c = 0.5206$ nm and Fm3m space group, which indicates it is $Ho_2Hf_2O_7$ phase. Due to the high stiffness of this kind of oxides, the formed $Ho_2Hf_2O_7$ phase could handicap the movement of dislocations and increase the strength [26]. In addition, the active Ho could promote the formation of specific oxide and dense oxide layer.

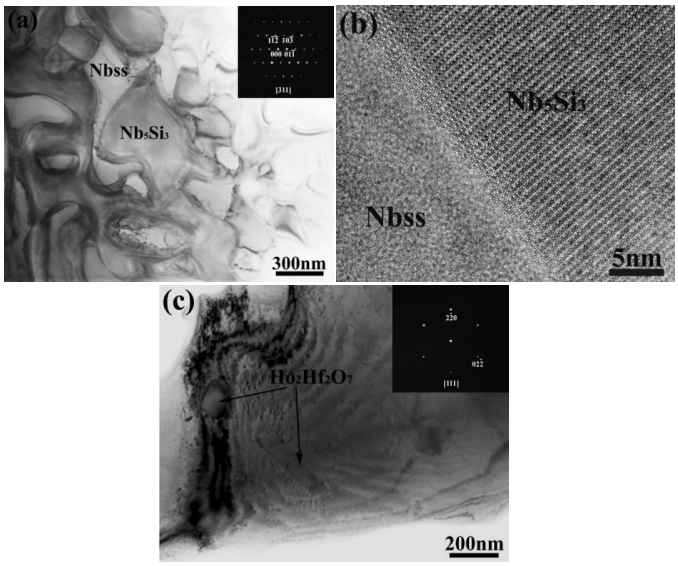

Fig. 3. TEM observations on the Nb-Si-Ti-Cr-Al-Ta-Hf alloy with 0.2 Ho addition: (a) Fine Nb/Nb_5Si_3 eutectic structure, (b) Morphology of $Ho_2Hf_2O_7$ particles (Inset images showing the SAED pattern of corresponding phases)

3.2. Compressive properties

The compression testes at different temperatures have been performed on the Nb-Si-Ti-Cr-Al-Ta-Hf alloys with different Ho additions and the results are shown in Fig. 4. Due to the presence of ductile-brittle transition of the NbSi based alloy, the compressive strain would be improved obviously with increased temperature, and only the compressive strain at room temperature is studied. As shown in Fig. 4(a), the room-temperature compressive strength and strain of the alloy without Ho addition are 1640 MPa and 12.5%, respectively. With 0.1 at.% Ho addition, the compressive strength and strain of the alloy are improved to 1825 MPa and 16.5%, respectively. When the Ho addition is increased to 0.2 at.%, the compressive properties are decreased a little with the compressive strength and strain of 1800 MPa and 16%, respectively. Generally, the minor Ho addition is beneficial to the compressive strength and strain, which should be mainly ascribed to the refined microstructure. With the test temperature increasing, the compressive strength of the alloy with different Ho addition has decreased

less than 20% at 873 K. The compressive strength of the Nb-Si-Ti-Cr-Al-Ta-Hf alloy with 0, 0.1 and 0.2 at.% Ho addition is about 1350 MPa, 1495 MPa and 1450 MPa, respectively. When the test temperature increases to 1273 K, the compressive strength of the Nb-Si-Ti-Cr-Al-Ta-Hf alloy with 0, 0.1 and 0.2 at.% Ho addition has an obvious drop and their values are 695 MPa, 765 MPa and 741 MPa, respectively. With the test temperature increasing to 1473 K, the compressive strength of the Nb-Si-Ti-Cr-Al-Ta-Hf alloy with 0, 0.1 and 0.2 at.% Ho addition has been decreased to 300 MPa, 380 MPa and 360 MPa, respectively. Comparatively, the compressive strength of the alloy has decreased gradually with the temperature. Especially at the temperature above 1273 K, the compressive strength drops significantly. Such a phenomenon could be attributed to the softening of the Nbss, which results in the decreased strength. The minor Ho addition improves the compressive strength at elevated temperature, which should be mainly attributed to the refined Nb_5Si_3 phase. The microstructure evolution could take full use of the strengthening phase and restrain the dislocation movement. In addition, the well distributed $Ho_2Hf_2O_7$ phases also benefits the strength by handicap the dislocation movement.

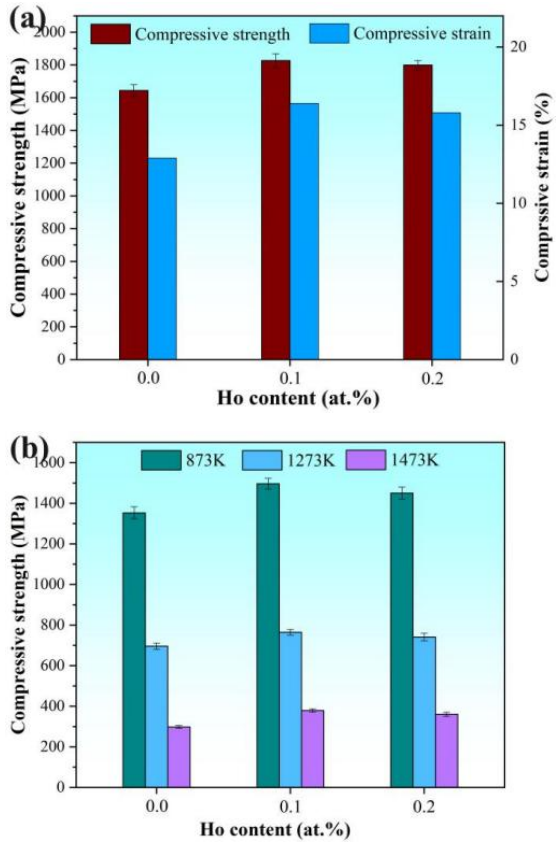

Fig. 4. Compressive properties of the Nb-Si-Ti-Cr-Al-Ta-Hf alloys with different Ho addition: (a) Compressive strength and strain at room temperature, (b) Compressive strength at elevated temperature

The typical cross-sectional microstructures of the Nb-Si-Ti-Cr-Al-Ta-Hf alloys with and without Ho addition after room-temperature compressive test have been observed and given in Fig. 5. It can be seen that the Nb_5Si_3 phases in the alloy without Ho addition have experienced great stress and almost crashed during the compression, as shown in Fig. 5(a). Moreover, the cracks could be observed in the Nbss matrix with similar propagating direction, which indicates the rapid stress transfer and less using of the ductile phase. In the Ho doped Nb-Si-Ti-Cr-Al-Ta-Hf alloy, the cracks with diversified propagating direction have distributed in the Nb_5Si_3 phases, as shown in Fig. 5(b). Moreover, there is almost no crack in the Nbss matrix. Such a feature indicates the stress has been changed by the synergistic deformation of Nbss and Nb_5Si_3 phases. Then, it can be concluded that the refined microstructure could well take advantage of the ductile and stiffness phases, which contributes to the strength and ductility simultaneously.

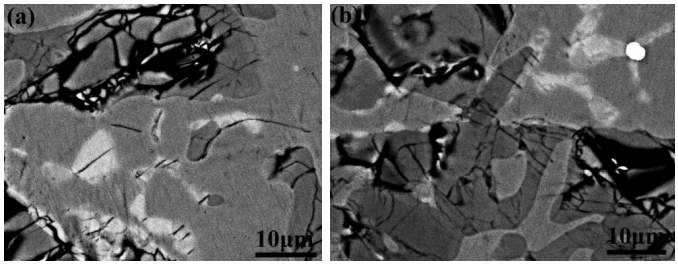

Fig. 5. SEM observations of the crack morphology in the Nb-Si-Ti-Cr-Al-Ta-Hf alloys with different Ho addition compressed at room temperature: (a) 0 Ho, (b) 0.1 Ho

3.3. Oxidation behavior

The oxidation behavior of the NbSi based alloy is an important issue, because of the "pest" oxidation phenomenon [15]. Though the Cr and Al addition could help to form the oxidation resistance surface layer, however, the rapid inner oxidation could destroy the protective layer. Actually, the active RE could induce the formation of specific oxide and help the oxidation resistance [27]. To study the effect of Ho addition on the oxidation behavior of the Nb-Si-Ti-Cr-Al-Ta-Hf alloy, the oxidation at 1373 K has been performed and mass variation of alloys is present in Fig. 6. Clearly, the Nb-Si-Ti-Cr-Al-Ta-Hf alloys with

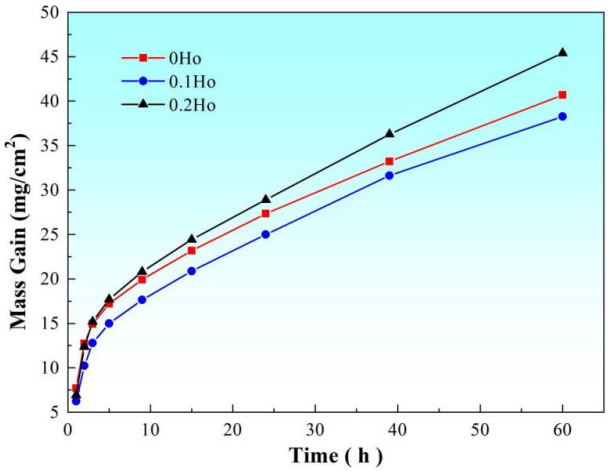

Fig. 6. Oxidation kinetics curves of the Nb-Si-Ti-Cr-Al-Ta-Hf alloys with different Ho addition at 1373 K

different Ho addition all demonstrate the increased mass with the time extending. Moreover, the mass variation curves exhibit the parabolic feature, which has rapid increasing rate at initial stage and then the increasing rate drops keeping at a certain value. Comparatively, the Nb-Si-Ti-Cr-Al-Ta-Hf alloy without Ho addition has the higher mass increasing at the initial stage, but it decreases a little in the following time and keeps at the medium value. The Nb-Si-Ti-Cr-Al-Ta-Hf alloy with 0.1 at.% Ho addition has the better oxidation behavior with the lowest mass increasing rate in all time. However, the 0.2 at.% Ho doped Nb-Si-Ti-Cr-Al-Ta-Hf alloy has the higher mass increasing rate at initial stage and the highest value in the following time.

The XRD analyses on the oxidized surfaces of Nb-Si-Ti-Cr-Al-Ta-Hf alloys with different Ho addition are shown in Fig. 7. It is clear that the high-temperature oxidation has resulted in complex oxides. Clearly, the surfaces of alloy are mainly composed of Nb_2O_5 based oxide. Due to the coexistence of Ti, and Ta elements in the Nb_5Si_3 and Ti_5Si_3 phases, the Nb_2O_5 almost forms with TiO_2 and Ta_2O_5 phases synergistically. Moreover, the diffraction peaks of $NbSi_2$ can be observed in the XRD patterns, which can be ascribed to the consumption of Nb during oxidation. With the consumption of Nb, the Nb content in the Nb_5Si_3 phase would be decreased, which leads to the transformation of Nb_5Si_3 to $NbSi_2$. In addition, the $AlNbO_4$ and $CrNbO_4$ also can be calibrated in the XRD patterns, which should be attributed to the solid solution of Al and Cr in Nbss matrix. Based on the XRD patterns, the Ho addition exerts little effect on the oxide types, except the formation of HfO_2 and $Ho_2Hf_2O_7$.

SEM observations on the oxidized surfaces are exhibited in Fig. 8. It can be found that the surface of Nb-Si-Ti-Cr-Al-Ta-Hf alloy without Ho addition is mainly covered by the rod-like phases with dual size, as shown in Fig. 8(a). The rod-like phases are intersected with each and there are some small particles interspersed inside. Moreover, the rod-like phases with different sizes prefer to aggregate separately. Combining with the XRD analyses, the rod-like phase should be Nb_2O_5 and the size may be related with the coordinated formed phase. With the 0.1 at.% Ho addition, the surface morphology has changed a little. As shown in Fig. 8(b), though the rod-like phase still has the high proportion, the size has decreased obviously, compared with those formed on the alloy without Ho addition. When the Ho addition increases to 0.2 at.%, the oxides are refined further, which almost changes the rod-like shape to small particles, as shown in Fig. 8(c). Furthermore, the micro-gaps could be observed in the oxidized surfaces, which indicates the relative loosening oxide film. However, the Ho addition could decrease the ratio of micro-gap with big size, which is helpful to improve the oxidation resistance.

To demonstrate the effect of Ho addition on the oxidation permeation, the cross-sectional microstructures of the Nb-Si-Ti-Cr-Al-Ta-Hf alloys with different Ho addition after oxidation have been characterized. As shown in Fig. 9, the Ho addition has really restrained the extending of oxidation in matrix. For the Nb-Si-Ti-Cr-Al-Ta-Hf alloy without Ho addition, the depth of inner oxidation zone is about 60 μm, as shown in Fig. 9(a). Moreover, the inner diffusion of oxygen has resulted in the oxidization

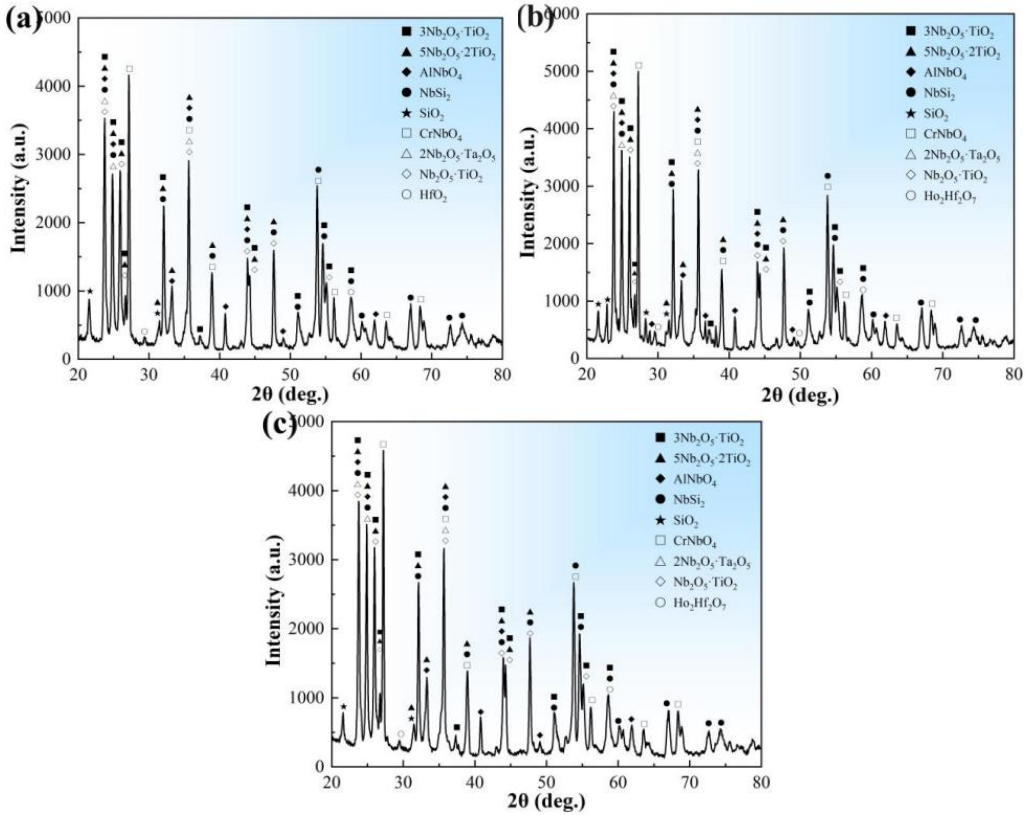

Fig. 7. X-ray diffraction patterns of Nb-Si-Ti-Cr-Al-Ta-Hf alloys with different Ho addition oxidized at 1373 K for 60 hours: (a) 0 Ho, (b) 0.1 Ho, (c) 0.2 Ho

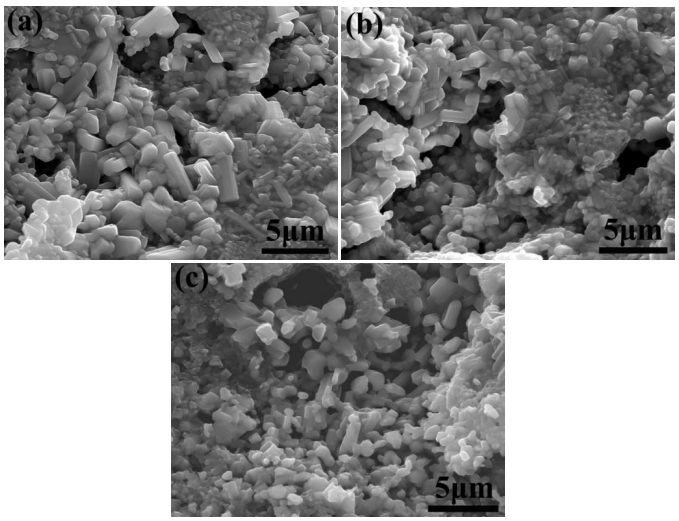

Fig. 8. SEM observations on the surfaces of Nb-Si-Ti-Cr-Al-Ta-Hf alloys with different Ho addition oxidized at 1373 K for 60 hours: (a) 0 Ho, (b) 0.1 Ho, (c) 0.2 Ho

along the Nbss/Nb_5Si_3 phase interface. With the addition of Ho, the depth of inner oxidation zone has been decreased, as shown in Fig. 9(b) and (c). The depth of inner oxidation zone of the Nb-Si-Ti-Cr-Al-Ta-Hf alloy with 0.1 and 0.2 at.% Ho addition is about 30 μm and 40 μm, respectively.

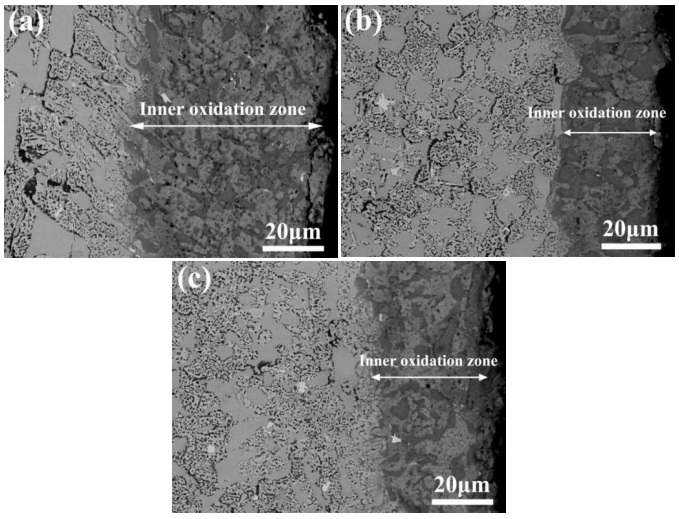

Fig. 9. SEM observations on cross-section of Nb-Si-Ti-Cr-Al-Ta-Hf alloys with different Ho addition oxidized at 1373 K for 60 hours: (a) 0 Ho, (b) 0.1 Ho, (c) 0.2 Ho

According to the recent researches [28-30], the mechanical properties are closely related with microstructure. Especially for the alloy with intermetallic phase, the ductile phase could play an important role [31,32]. In the present research, the Nbss acts as the ductile phase to improve the room-temperature deformation behavior of the NbSi based alloy. The original multi-phase structure in Nb-Si-Ti-Cr-Al-Ta-Hf alloy could use the Nb_5Si_3 phase to enhance the strength, but it could not take full use of the Nbss phase to improve the ductility. Due to the coarse microstructure, the propagation of microcracks initiated in Nb_5Si_3 would be accelerated inside and difficult to be bridged or reversed by the Nbss phase [33]. The Ho addition refines the microstructure and suppresses the rapid propagation of crack along linear direction, which contributes to the compressive ductility. Therefore, the Nb-Si-Ti-Cr-Al-Ta-Hf alloy with Ho addition has better compressive strength and strain simultaneously. Due to the high activity of RE, the doped Ho could induce the selective oxidation along phase interface and restrain the inner diffusion of oxygen. Therefore, the 0.1 at.% Ho doped Nb-Si-Ti-Cr-Al-Ta-Hf alloy possesses the best oxidation resistance. If more Ho is added, it would accelerate the oxidation and begin to extend the inner oxidation, which is detrimental to the oxidation resistance. Then, the appropriate Ho addition is helpful to regulate the micostructure of the Nb-Si-Ti-Cr-Al-Ta-Hf alloy and improve its properties.

4. Conclusions

In the present research, the Nb-Si-Ti-Cr-Al-Ta-Hf alloys with different Ho addition were prepared. Their microstructure, compressive properties and oxidation behaviors were studied preliminarily. Some conclusions can be drawn as following.

(1) The Nb-Si-Ti-Cr-Al-Ta-Hf alloy prepared by vacuum arc smelting possesses coarse microstructure which is mainly composed of Nb solid solution, Nb_5Si_3 and Ti_5Si_3 phases. The minor Ho addition could refine the microstructure and suppress the precipitation of Ti_5Si_3 phase. Moreover, the Ho addition also results in the formation of $Ho_2Hf_2O_7$, which prefers to precipitate along the Nbss/Nb_5Si_3 phase interface.

(2) Compared with the Nb-Si-Ti-Cr-Al-Ta-Hf alloy, the minor Ho addition improves the room-temperature and high-temperature compressive properties. Its room-temperature compressive strength and ductility obtain the maximum value of 1825 MPa and 16.5% when the Ho content is 0.1 at.%. Moreover, the alloy with 0.1 at.% Ho has the best compressive strength at 873 K, 1273 K and 1473K with value of 1495 MPa, 765 MPa and 380 MPa, respectively.

(3) The oxidation behavior of the Nb-Si-Ti-Cr-Al-Ta-Hf alloy is diversified with the Ho addition. The oxidation rate of the alloy with 0.1 at.% Ho addition is the lowest while the alloy with 0.2 at.% Ho addition is the highest. Therefore, the 0.1 at.% Ho would be the appropriate content for the Nb-Si-Ti-Cr-Al-Ta-Hf alloy.

Acknowledgments

The authors gratefully acknowledge the support provided by the Guangdong Basic and Applied Basic Research Foundation (2020A1515011301), Shenzhen Basic Research Project (JCYJ20210324120001003, JCYJ20200109144604020, and JCYJ20200109144608205) and the IER Foundation (IERF202102, IERF202201, and IERF202202).

REFERENCES

[1] L.Y. Sheng, F. Yang, T.F Xi, J.T. Guo, J. Alloys Compd. **554**, 182-188 (2013).

[2] Q.L. Wang, R. Li, W.X. Xie, F. Yang, B.N. Du, L.Y. Sheng, Mater. **16**, 3362 (2023).

[3] B.P. Bewlay, M.R. Jackson, P.R. Subramanian, J.C. Zhao, Metall. Mater. Trans. A **34**, 2043-52 (2003).

[4] L.Y. Sheng, F. Yang, T.F. Xi, J.T. Guo, H.Q. Ye, Mater. Sci. Eng. A **555**, 131-8 (2012).

[5] B.N. Du, L.Y. Sheng, Z.Y. Hu, C.Y. Cui, J.X. Yang, X.F. Sun, Adv. Mech. Eng. **10**, 1-8 (2018).

[6] Y.T. He, X.H. Zhu, C.X. Zhang, Z.Q .Liu, B.B. Cao, L.Y. Sheng, Y. Yang, Q.G. Feng, N. Wang, J.Z. Ou, Y. Xu, ACS Sustainable Chem. Eng. **11**, 5055-64 (2023).

[7] Y.W. Yang, H.Y. Zhao, Z.Y. Yin, J.Q. Zhao, X.T. Yin, N. Li, D.D. Yin, Li Y. Nan, B. Lei, Y.P. Du, W.X. Que, Surf. Innovations **7**, 4-9(2019).

[8] Y.M. Li, G.R. Zhao, H. Qi, M.S. Li, Y.F. Zheng, Y.H. Qian, L.Y. Sheng, Ceram. Int. **44,** 17530-34 (2018).

[9] H. Zhao, C.C. Zhao, W.X. Xie, D. Wu, B.N. Du, X.R. Zhang, M. Wen, R. Ma, R. Li, J.K. Jiao, C. Chang, X.C. Yan, L.Y. Sheng, Mater. **16**, 3250 (2023).

[10] A. Suzuki, T.M. Pollock, Acta Mater. **56**, 1288-97 (2008).

[11] L.Y. Sheng, Y.X. Tian, J.T. Guo, Adv. Compo. Lett. **27**, 168-175 (2018).

[12] Y.X. Tian, J.T. Guo, L.Y. Sheng, G.M. Cheng, L.Z. Zhou, L. He, H.Q. Ye, Intermetallics **16**, 807-12 (2008).

[13] B.P. Bewlay, M.R. Jackson, J.C. Zhao, P.R. Subramanian, M.G. Mendiratta, J.J. Lewandowski, MRS Bull. **28**, 646-53 (2003).

[14] Y. Pan, Y.H. Lin, H. Wang, C.M. Zhang, Mater. Des. **86**, 259-65 (2015)

[15] Y. Li, B. Gan, Z.N. Bi, H.Y. Yu, C.G. Zhou, J.B. Sha, Corros. Sci. **187**, 109513 (2021)

[16] S. Zhang, X.P. Guo, Intermetallics **70**, 33-44 (2016).

[17] Y.X. Tian, J.T. Guo, G.M. Cheng, L.Y. Sheng, L.Z. Zhou, L.L. He, H. Ye, Mater. Des. **30**, 2274-77 (2009).

[18] S.Y. Qu, Y.F. Han, L.G. Song, Intermetallics **15**, 810-813 (2007).

[19] Z. Li, L.M. Peng, Acta Mater. **55**, 6573-85 (2007).

[20] I. Grammenos, P. Tsakiropoulos, Intermetallics **18**, 242-53 (2010).

[21] L.Y. Sheng, Y. Xie, T.F. Xi, J.T. Guo, Y.F. Zheng, H.Q. Ye, Mater. Sci. Eng. A **528**, 8324-31 (2011).

[22] L.Y. Sheng, F. Yang, T.F. Xi, Y.F. Zheng, J.T. Guo, Intermetallics **27**, 14-20 (2012).

[23] L. Sheng, W. Zhang, J. Guo, H. Ye, Mater. Charact. **60** 1311-16 (2012).

[24] B.N. Du, Z.P. Xiao, Y.X. Qiao, L. Zheng, B.Y. Yu, D.K. Xu, L.Y. Sheng, J. Alloys Compd. **775**, 990-1001 (2019).

[25] G.M. Cheng, Y.X. Tian, L.L. He, J.T. Guo, Philos. Mag. **89**, 2801-12 (2009).

[26] L. Zheng, L. Sheng, Y. Qiao, Y. Yang, C. Lai, Mater. Res. Express **6**, 046502 (2019).

[27] Y. Tan, H. Fang, R. Chen, Y. Liu, Y. Su, J. Guo, H. Cui, S. Zhang, H. Fu, Intermetallics **126**, 106883 (2020).

[28] X. Xiao, X. Le, Z. Chao, L.Y. Sheng, Y.A. Guo, L.Z. Zhou, Adv. Mater. Res. **452**, 51-55(2012). .

[29] Y. Chao, Y. Liu, Z. Xu, W. Xie, L. Zhang, W. Ouyang, H. Wu, Z. Pan, J. Jiao, S. Li, G. Zhang, W. Zhang, L. Sheng, J. Mater. Sci. Technol. **156**, 32-53 (2023).

[30] J. Wang, L. Meng, W. Xie, C. Ji, R. Wang, P. Zhang, L. Jin, L.Y. Sheng, Y. Zheng, J. Magnesium Alloys (2022). DOI: https://doi.org/10.1016/j.jma.2022.09.025

[31] W. Liu, S. Huang, L. Jia, Y. Kang, J. Sha, B. Chen, Y. Wu, H. Xiong, J. Mater. Sci. Technol. **149**, 127-53 (2023).

[32] L. Sheng, J. Guo, W. Zhang, L. Zhou, H. Ye, Int. J. Mater. Res. **100**, 1602-06 (2009).

[33] J.M. Yang, S.M. Jeng, K. Bain, R.A. Amato, Acta Mater. **45**, 295-305 (1997).